Article

Maternal inheritance of glucose intolerance via oocyte TET3 insufficiency

https://doi.org/10.1038/s41586-022-04756-4

Received: 3 August 2020

Accepted: 12 April 2022

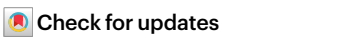

Bin Chen[1,2,3,11], Ya-Rui Du[3,11], Hong Zhu[4,5,11], Mei-Ling Sun[3,6,11], Chao Wang[3,6,11], Yi Cheng[4,5], Haiyan Pang[1], Guolian Ding[4,5], Juan Gao[3], Yajing Tan[7], Xiaomei Tong[2], Pingping Lv[1], Feng Zhou[2], Qitao Zhan[1], Zhi-Mei Xu[3], Li Wang[7], Donghao Luo[2], Yinghui Ye[1], Li Jin[4,5], Songying Zhang[2], Yimin Zhu[1], Xiaona Lin[2], Yanting Wu[4,5], Luyang Jin[1], Yin Zhou[8], Caochong Yan[1], Jianzhong Sheng[1], Peter R. Flatt[9], Guo-Liang Xu[3,10]✉ & Hefeng Huang[1,4,5,7]✉

Diabetes mellitus is prevalent among women of reproductive age, and many women are left undiagnosed or untreated[1]. Gestational diabetes has profound and enduring effects on the long-term health of the offspring[2,3]. However, the link between pregestational diabetes and disease risk into adulthood in the next generation has not been sufficiently investigated. Here we show that pregestational hyperglycaemia renders the offspring more vulnerable to glucose intolerance. The expression of TET3 dioxygenase, responsible for 5-methylcytosine oxidation and DNA demethylation in the zygote[4], is reduced in oocytes from a mouse model of hyperglycaemia (HG mice) and diabetic humans. Insufficient demethylation by oocyte TET3 contributes to hypermethylation at the paternal alleles of several insulin secretion genes, including the glucokinase gene (*Gck*), that persists from zygote to adult, promoting impaired glucose homeostasis largely owing to the defect in glucose-stimulated insulin secretion. Consistent with these findings, mouse progenies derived from the oocytes of maternal heterozygous and homozygous *Tet3* deletion display glucose intolerance and epigenetic abnormalities similar to those in the oocytes of HG mice. Moreover, the expression of exogenous *Tet3* mRNA in oocytes from HG mice ameliorates the maternal effect in offspring. Thus, our observations suggest an environment-sensitive window in oocyte development that confers predisposition to glucose intolerance in the next generation through TET3 insufficiency rather than through a direct perturbation of the oocyte epigenome. This finding suggests a potential benefit of pre-conception interventions in mothers to protect the health of offspring.

Diabetes mellitus is a widespread major public health issue; however, efforts to prevent and treat diabetes mellitus have shown limited success[1,5]. Prolonged hyperglycaemia in diabetes increases the risk of multisystemic complications[1]. Maternal hyperglycaemia confers long-term complications to offspring and has a profound impact on public health[6–8]. Maternal environmental factors, including adverse germline or in utero exposure, caring behaviours and milk composition[9–11], reprogramme the health of offspring across generations through intergenerational or transgenerational epigenetic inheritance[10,12–15]. Although epigenetic inheritance in mammals via gametes has been reported[14,16–19], the mechanism of female germline-dependent epigenetic inheritance remains largely unclear. Here, we sought to determine how the long-term health of offspring is affected by pregestational hyperglycaemia.

Oocyte-transmitted glucose intolerance

To ensure that the phenotypes of mouse progenies originated exclusively from the oocyte, we performed in vitro fertilization (IVF) and 2-cell embryo transfer to foster mothers to produce offspring (Fig. 1a). The oocyte donors—streptozotocin (STZ)-induced HG females—displayed gradually increased blood glucose levels (Extended Data Fig. 1a). Although the number of MII oocytes retrieved was markedly reduced in the HG group compared with the control (Extended Data Fig. 1b–e),

[1]Key Laboratory of Reproductive Genetics (Ministry of Education), Department of Reproductive Endocrinology, Women's Hospital, Zhejiang University School of Medicine, Hangzhou, China. [2]Assisted Reproduction Unit, Department of Obstetrics and Gynecology, Sir Run Run Shaw Hospital, School of Medicine, Zhejiang University, Key Laboratory of Reproductive Dysfunction Management of Zhejiang Province, Hangzhou, China. [3]State Key Laboratory of Molecular Biology, Shanghai Key Laboratory of Molecular Andrology, Shanghai Institute of Biochemistry and Cell Biology, Center for Excellence in Molecular Cell Science, Chinese Academy of Sciences, Shanghai, China. [4]Obstetrics and Gynecology Hospital, Institute of Reproduction and Development, Fudan University, Shanghai, China. [5]Research Units of Embryo Original Diseases, Chinese Academy of Medical Sciences, Shanghai, China. [6]University of Chinese Academy of Sciences, Beijing, China. [7]Shanghai Key Laboratory of Embryo Original Diseases, International Peace Maternity and Child Health Hospital, School of Medicine, Shanghai Jiao Tong University, Shanghai, China. [8]Center for Reproductive Medicine, The Second Affiliated Hospital, School of Medicine, Zhejiang University, Hangzhou, China. [9]Centre for Diabetes Research, School of Biomedical Sciences, Ulster University, Coleraine, UK. [10]Shanghai Key Laboratory of Medical Epigenetics, Institutes of Biomedical Sciences, Medical College of Fudan University, Shanghai, China. [11]These authors contributed equally: Bin Chen, Ya-Rui Du, Hong Zhu, Mei-Ling Sun, Chao Wang. ✉e-mail: glxu@sibcb.ac.cn; huanghefg@fudan.edu.cn

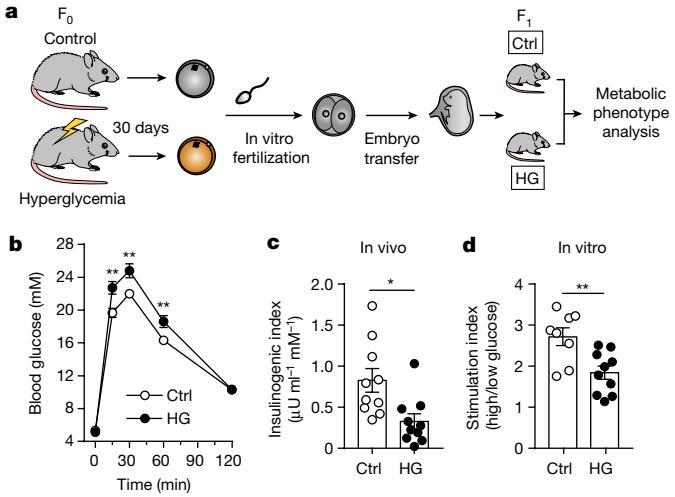

Fig. 1 | Pregestational hyperglycaemia leads to glucose intolerance in offspring. a, Schematic of the nongenetic maternal hyperglycaemia model and offspring breeding. The lightning denotes chemical treatment to generate F_0 hyperglycaemia. Ctrl, control. **b**, Glucose tolerance test (GTT) results for male offspring at 16 weeks of age. Ctrl: $n = 16$ mice, HG: $n = 12$ mice. **c**, Insulinogenic index during the GTT of male offspring at 16 weeks of age. $n = 10$ mice per group. **d**, The stimulation index of insulin release from isolated pancreatic islets of male offspring at 16 weeks of age. Ctrl: $n = 8$ mice, HG: $n = 10$ mice. **b**–**d**, Data are mean ± s.e.m.; two-tailed *P*-values were calculated by one-way repeated-measurements ANOVA followed by post hoc unpaired *t*-test (**b**) or unpaired Student's *t*-test (**c**, **d**). $^*P < 0.05$, $^{**}P < 0.01$. Statistical details are in Supplementary Table 5.

the embryonic developmental competence and litter size were not altered following IVF and embryo transfer (Extended Data Fig. 1f–k). The offspring derived from the HG females also exhibited normal growth and body weight compared with the controls (Extended Data Fig. 2a).

To examine the metabolic state of the F_1 offspring from HG mothers, we tested glucose tolerance in cohorts from 8 weeks to 2 years of age. Male offspring exhibited higher blood glucose levels after glucose injection from 16 weeks of age onwards, whereas females had higher blood glucose from 1 year of age (Fig. 1b, Extended Data Fig. 2b–f). These longitudinal observations of metabolic effects indicate that both male and female HG offspring gradually exhibited overt glucose intolerance compared with controls from a lifetime perspective, although the females exhibited delayed onset compared with males, presumably owing to the protective effect of sex hormones[20]. These data demonstrate that impaired glucose tolerance, a prediabetes status, appeared in the HG offspring. To confirm that HG offspring were more susceptible to diabetes, we fed all offspring with a calorie-dense high-fat research diet (HFD) to induce insulin resistance and accelerate the progression of diabetes[21,22]. After induction with HFD, the body weight did not differ between HG and non-HG two groups (Extended Data Fig. 2g), whereas both male and female offspring in the HG group showed glucose intolerance earlier, from 12 weeks of age onwards (Extended Data Fig. 2h–j). Together, these data demonstrate that F_1 offspring from HG mothers tend to show a glucose intolerance phenotype in a sexually dimorphic manner, most prominently among the males and older mice of both sexes.

To investigate the persistence of the transgenerational effect mediated via the germline, we generated F_2 mice by inter-crossing control and HG F_1 mice (Extended Data Fig. 3a). Compared with those with control F_1 parents, the F_2 offspring with a F_1 HG father and/or mother did not exhibit glucose intolerance at 24 weeks of age (Extended Data Fig. 3b, c). These data suggest that the effects of maternal pregestational hyperglycaemia might extend only to the immediate offspring and are unlikely to persist to the second generation.

To determine the primary defect in the glucose intolerance, we measured insulin sensitivity and insulin secretion in the F_1 offspring. As insulin sensitivity in HG offspring was similar to that in controls under both normal conditions and with HFD challenge (Extended Data Fig. 4a–d), glucose intolerance in HG offspring was probably a result of dysfunctional insulin secretion. The insulin secretory function of pancreatic β-cells was therefore assessed at the initial diagnosis of glucose intolerance among offspring. During the glucose tolerance test, the serum insulin response to glucose in HG males was reduced during the first 30 min after the glucose load (Fig. 1c). An in vitro glucose-stimulated insulin secretion (GSIS) test using pancreatic islets isolated from the HG mice demonstrated an impaired acute insulin secretory response to glucose over basal compared with that observed with islets from the control group (Fig. 1d, Extended Data Fig. 4e), whereas the morphology of pancreatic islets or insulin content did not differ between male offspring of the two groups (Extended Data Fig. 4f–l). These data suggest that pregestational hyperglycaemia leads primarily to defective insulin secretion in offspring.

Insufficient oocyte TET3 at high glucose

As the mammalian epigenome is properly reprogrammed by various epigenetic modifying factors between generations in mammals[23], maternal environmental exposure might perturb the epigenetic reprogramming of gametes and early embryos, and thus increase the disease susceptibility of offspring[13,24,25]. To identify the potential epigenetic modifiers that mediate the female germline-dependent epigenetic inheritance, we performed RNA sequencing (RNA-seq) on HG MII oocytes (Supplementary Table 1). Among the key epigenetic modifiers expressed in MII oocytes (with fragments per kilobase per million (FPKM) >20 in controls), *Tet3* was noted for its high abundance and significant reduction of the transcription level in the HG group (Fig. 2a, b, Extended Data Fig. 5a–d). A reduction of *Tet3* expression by almost 50% in HG MII oocytes was verified using quantitative PCR with reverse transcription (RT–qPCR) (Extended Data Fig. 5e). Moreover, in another hyperglycaemic mouse model of obesity (referred to as the type 2 diabetes (T2DM), *Tet3* mRNA was also reduced in germinal vesicle (GV) oocytes (Extended Data Fig. 5f, g). TET3 is the only DNA 5-methylcytosine (5mC)-modifying enzyme expressed during oocyte development that catalyzes the conversion of 5mC to 5-hydroxymethylcytosine (5hmC) and other high-oxidation products, with an essential role in DNA demethylation at the zygote stage, especially in the male pronucleus[4,26–28]. Immunofluorescence staining confirmed that IVF-derived pronucleus stage 3–4 (PN3–4) zygotes from HG females exhibited markedly reduced TET3 signals and 5hmC/5mC ratios mainly in the male pronucleus (Extended Data Fig. 5h–k). These observations suggest that TET3 is reduced in oocytes in response to maternal hyperglycaemia, with insufficient zygotic DNA demethylation as a consequence.

Moreover, in oocytes from STZ-treated donor mice with different blood glucose levels (Extended Data Fig. 6a), *Tet3* mRNA levels were found to be downregulated in a glucose concentration-dependent manner at both GV and MII stages (Fig. 2c). Notably, STZ-treated mice with normoglycaemia did not show altered levels of *Tet3* transcript in oocytes (Fig. 2c). Next, we tested whether the extracellular environment of HG oocytes had a higher glucose concentration. Owing to the insufficient volume of mouse follicular fluid, we used a hyperglycaemic rat model. Indeed, a much higher concentration of glucose was detected in the follicular fluid of hyperglycaemic rats (Extended Data Fig. 6b). Given that an in vivo high-glucose environment increases glucose accumulation in oocytes[29], we reasoned that decreased *Tet3* expression might result from the exposure to high environmental glucose. As expected, treatment with high glucose led to a reduction of *Tet3* expression both in mouse oocytes within follicles under in vitro growth (IVG) and in oocytes under in vitro maturation (IVM) (Extended Data Fig. 6c, d). Notably, *Tet3* expression

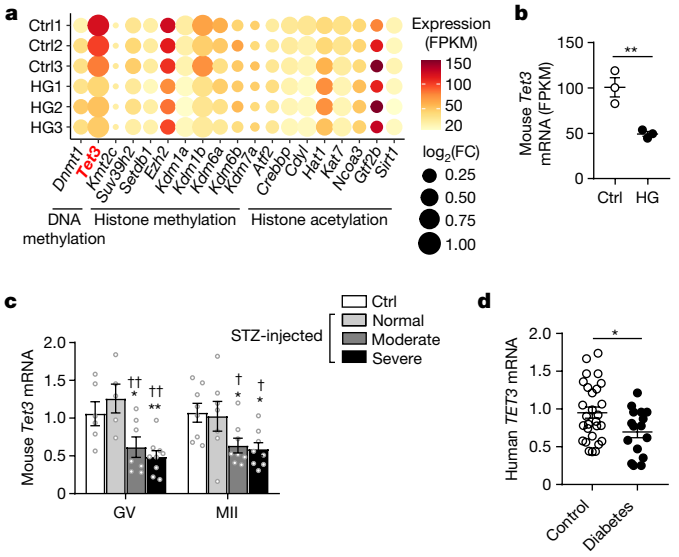

Fig. 2 | Decreased TET3 expression in oocytes from hyperglycaemic mouse and diabetic human. a, Bubble plot showing gene expression of key epigenetic modifiers (FPKM >20) in HG versus control groups based on RNA-seq analysis of mouse MII oocytes from 3 biological replicates. For each replicate, ten oocytes were collected from a mouse. The colour and size of the dots denote the expression level (FPKM) and the absolute value of $\log_2$-transformed fold change (FC), respectively. *Tet3* is notable for its high abundance and fold change. **b**, *Tet3* mRNA expression in mouse oocytes, determined by RNA-seq analysis in Fig. 2a. **c**, *Tet3* mRNA expression in mouse oocytes, measured by RT–qPCR in the Ctrl group and STZ-treated groups with normoglycaemia (normal), moderate hyperglycaemia (moderate) and severe hyperglycaemia (severe). $n = 6$ (Ctrl), 5 (normal), 7 (moderate) and 9 (severe) replicates for GV oocytes; 8 (Ctrl), 7 (normal), 8 (moderate) and 8 (severe) replicates for MII oocytes (with 10 oocytes pooled from 1–3 mice for each replicate). *Comparison with Ctrl; †comparison with normoglycaemia. **d**, *TET3* mRNA expression in GV oocytes from diabetic humans ($n = 16$ oocytes from 8 individuals) and from paired nondiabetic controls ($n = 28$ oocytes from 16 individuals). Data are mean ± s.e.m. (**b**–**d**); two-tailed *P*-values by unpaired Student's *t*-test (**b**, **d**) or one-way ANOVA with post hoc least significant difference multiple comparisons (**c**). $^{*}P < 0.05$, $^{**}P < 0.01$, $^{\dagger}P < 0.05$, $^{\dagger\dagger}P < 0.01$. Statistical details are in Supplementary Table 5.

in the oocytes cultured in media with normal physiological D-glucose supplemented with high L-glucose was similar to that in oocytes from the normal D-glucose concentration group (Extended Data Fig. 6c, d). As L-glucose is not physiologically active, these data indicate that down-regulation of *Tet3* in the oocytes can be attributed to glucose metabolism rather than physical factors such as high osmolality. Furthermore, *Tet3* mRNA appeared to be more susceptible to degradation when the mouse oocytes were exposed to high glucose (Extended Data Fig. 6e, f). Similarly, follicular fluid from diabetic women also showed increased glucose levels (Extended Data Fig. 6g), and GV oocytes from hyperglycaemic women with diabetes had reduced *TET3* expression compared with those from paired nondiabetic women (Fig. 2d, Supplementary Table 2). When immature oocytes obtained from euglycaemic patients were cultured for IVM, *TET3* expression in MII oocytes was significantly reduced with higher glucose concentrations in the media (comparing 10 mM and 15 mM to 2.5 mM) (Extended Data Fig. 6h, Supplementary Table 2). Collectively, these data suggest that *Tet3* expression is compromised by high glucose in both human and mouse oocytes in vivo and in vitro.

Hypermethylation of β-cell genes

Considering the reduction of *Tet3* expression and the impaired DNA hydroxylation in HG zygotes, we next searched for aberrantly methylated genes conferring glucose intolerance by characterizing the methylome of the fetal mouse pancreatic islets on embryonic day 18.5 (E18.5) by whole-genome bisulfite sequencing (WGBS) (Supplementary Table 3). As a deficit in TET3-mediated demethylation usually leads to a high level of DNA methylation in certain regions, we examined the differentially methylated regions with hypermethylation (hyper-DMRs) (Extended Data Fig. 7a–c). Since promoter methylation is inversely correlated with transcription[30,31], we focused on DMRs at promoters. Notably, genes with hyper-DMRs at the promoter were enriched in the insulin secretion pathway (Fig. 3a, Extended Data Fig. 7d). This result is in agreement with the defective GSIS observed in HG offspring. Among these insulin secretion genes, *Gck*—with a hyper-DMR located in the pancreas-specific promoter (Fig. 3b)—encodes the rate-limiting glucokinase enzyme that regulates GSIS and acts as an essential component of the glucose-sensing machinery in pancreatic β-cells[32–35]. As previously reported, compromised *Gck* expression or function contributes to the dysfunction of β-cells[36–41] and increased DNA methylation at *GCK* is also regarded as a predictor of type 2 diabetes[42]. Together, the pathway enrichment analysis of genes with promoter hyper-DMRs points to a link between the glucose intolerance associated with defective insulin secretion in HG offspring and impaired demethylation due to TET3 insufficiency in oocytes.

To determine whether the affected methylation modification originates from early maternal exposure to impair GSIS in offspring, we traced the methylation pattern on the *Gck* promoter during mouse development. To examine the association between hypermethylation of the *Gck* promoter and the deficit of TET3-mediated active demethylation, we analysed the levels of 5mC and its oxidative product 5hmC in zygotes in which the passive demethylation was inhibited by the DNA replication inhibitor aphidicolin. Combined bisulfite sequencing and APOBEC-coupled epigenetic (ACE) sequencing analyses of male pronuclei from IVF-derived PN3–4 zygotes showed that the 5′ region of LINE-1 transposons, which are actively demethylated by TET3 in the zygotic male pronucleus[4], exhibited a higher methylation level in the HG group, indicating impaired active demethylation in HG male pronuclei (Extended Data Fig. 8a, b). Notably, the *Gck* promoter in the PN3–4 zygotes of HG group also had significantly more methylation but less hydroxymethylation than the control group (with 5mC and 5hmC levels of 79.3% and 3.6%, respectively, in the HG group compared with 57.8% and 7.1%, respectively, in the control group) (Fig. 3c, Extended Data Fig. 8c, d). A higher level of methylation (with a combined 5mC and 5hmC level of 69.3% in the HG group compared with 45% in the control group) was also detected on the paternal *Gck* allele in the late zygote at pronuclear stage 5, using a strategy based on a 35-bp deletion before of the promoter to track the paternal allele (Extended Data Fig. 8e, f). The increased methylation levels at the *Gck* promoter were further detected in HG samples of blastocyst stage embryos (Fig. 3d), E18.5 fetal islets (Fig. 3e) and pancreatic islets in offspring at 3 weeks (Extended Data Fig. 8g, h) and 16 weeks (Extended Data Fig. 8i, j), indicative of the persistence of hypermethylation throughout development. Consistent with the promoter hypermethylation (Extended Data Fig. 8k), mRNA expression of *Gck*—as well as several other hypermethylated genes involved in insulin secretion—as reduced in HG pancreatic islets compared with controls (Fig. 3f, Extended Data Fig. 8l, m). Involvement of disturbances of GCK in defective GSIS was supported by the observations that the GCK activator dorzagliatin improved glucose tolerance in the HG mice and increased GSIS from their islets when incubated in vitro (Extended Data Fig. 8n, p). To verify whether similar hypermethylation occurs in human patients, we assessed DNA methylation at the *GCK* promoter in in vitro cultured blastocysts from a human couple in which the woman had diabetes (diabetes group) and from two couples without diabetes (control). The amount of methylation at the *GCK* promoter was higher in the blastocyst from the diabetes group than from the control group (Fig. 3g, Supplementary Table 2). These data imply that hyperglycaemia might initiate epigenetically inheritable hypermethylation at the *GCK*

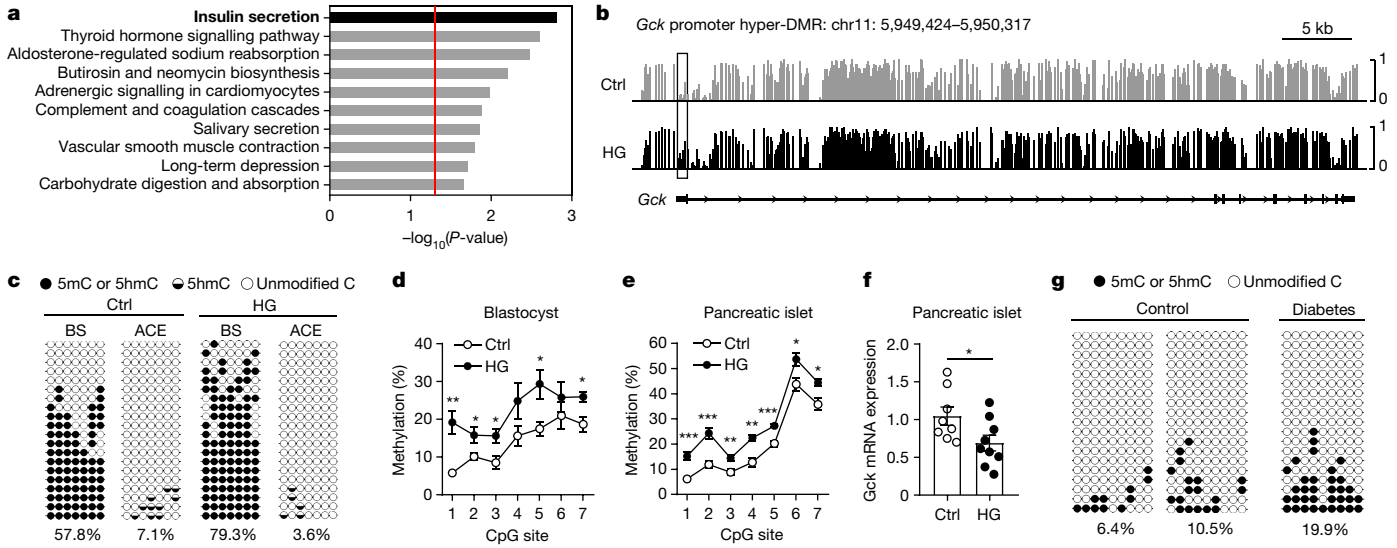

Fig. 3 | Pregestational hyperglycaemia alters DNA methylation at genes controlling insulin secretion in mouse offspring and human blastocysts. **a**, Top pathways identified from KEGG analysis of genes with hyper-DMRs in their promoter region. Hyper-DMRs were determined on the basis of the WGBS data of HG E18.5 mouse fetal islets. The red line corresponds to $P = 0.05$. **b**, Methylation profile of the *Gck* gene. Vertical bars (Ctrl, grey; HG, black) above the horizontal line indicate the methylation level (0–1) at individual CpG dyads (counting the two complementary CpGs). The box indicates a hyper-DMR in the pancreas-specific promoter. **c**, Bisulfite sequencing (BS) and ACE sequencing analyses of the *Gck* promoter in male pronuclei isolated from aphidicolin-treated PN3–4 mouse zygotes. The percentages of methylated CpGs are indicated. **d**, **e**, Pyrosequencing analysis of the *Gck* promoter methylation in mouse blastocysts (**d**) and E18.5 pancreatic islets (**e**). Ctrl and HG: $n = 6$ replicates per group (with 5 blastocysts pooled for each replicate) for blastocysts; $n = 9$ (Ctrl) and 7 (HG) mice for fetal islets. **f**, *Gck* mRNA expression of 8-week-old male pancreatic islets. Ctrl, HG: $n = 8$ and 9 mice. **g**, Bisulfite sequencing analysis of the *GCK* promoter in human blastocysts from two nondiabetic control couples ($n = 3$ blastocysts per couple) and from one couple with a diabetic female ($n = 4$ blastocysts). The percentages of methylated CpGs are indicated. *P*-values by Fisher's exact test (**a**). Data are mean ± s.e.m. (**c**–**f**); two-tailed *P*-values by unpaired Student's *t*-test. $^{*}P < 0.05$, $^{**}P < 0.01$ and $^{***}P < 0.001$. Statistical details are in Supplementary Table 5.

promoter, which in turn interferes with gene expression, leading to glucose intolerance in the next generation.

Our results strongly suggest that altered DNA methylation associated with an increased susceptibility to metabolic impairments arises from insufficient TET3-mediated demethylation and is heritable to a large extent, as exemplified by the *Gck* gene. To further examine the parental origin of *Gck* promoter hypermethylation, the paternal allele was tracked by the presence of a 35-bp deletion before the promoter in blastocysts (Extended Data Fig. 8e). Pyrosequencing analysis revealed that *Gck* promoter hypermethylation is specific to the paternal allele in the HG blastocysts (Extended Data Fig. 9a–c). This result suggests that the *Gck* hypermethylation originates from the male pronucleus rather than emerging during embryo development. To trace the parental origin of all the hypermethylated insulin secretion genes at the fetal stage, we analysed allele-specific 5mC distribution using single nucleotide polymorphism (SNP) based on the WGBS data. Among the nine genes with promoter hyper-DMRs of the insulin secretion pathway in HG E18.5 fetal islets, SNPs were available for five genes to distinguish the parental origin of sequences in the hyper-DMR region. Notably, the promoter of four genes, including *Gck*, *Rapgef4*, *Gna11* and *Prkca*, exhibited hypermethylation specific to the paternal allele (Extended Data Fig. 9d). This result suggests that more genes—besides *Gck*—are affected by oocyte TET3 insufficiency. Together, these results indicate that paternal hypermethylation persists in a subgroup of genes of the insulin secretion pathway and is probably traceable to oocyte TET3 insufficiency.

Transgenerational effect evoked by TET3

To further confirm that TET3 insufficiency causes increased susceptibility to diabetes in offspring, we used female mice with *Tet3* alleles floxed for the deletion of exon 8–9—which encode part of the catalytic domain[4]—to generate embryos and offspring of the three test groups by mating them with wild-type males (Extended Data Fig. 10a, b). To verify that *Gck* promoter hypermethylation in the offspring is attributable to insufficient TET3-mediated demethylation in the one-cell embryo, the *Gck* methylation level was determined in male pronuclei isolated from IVF-derived PN3–4 zygotes from maternal *Tet3*-knockout (Mat-KO), maternal *Tet3*-heterozygous (Mat-Het) and maternal wild-type (Mat-WT) groups of mice (Extended Data Fig. 10a, b). In zygotes with wild-type maternal TET3, substantial demethylation occurred by the PN3–4 stage, as reflected by the difference in methylation levels (96.4% in the sperm versus 62.1% in the male pronuclei). In the absence of maternal TET3, the zygotic *Gck* paternal allele remained largely hypermethylated (90% in Mat-KO male pronuclei versus 96.4% in sperm) (Fig. 4a). Of note, a significant impediment in demethylation was also observed in zygotes with a heterozygous deficiency of maternal TET3, as evidenced by a methylation retention rate of 85%, consistent with diminished 5hmC production (5% compared to 11.4% in the wild type) (Fig. 4a, Extended Data Fig. 10c–e). The *Gck* hypermethylation state persisted through the blastocysts to E18.5 fetal islets (Fig. 4b, c) and 3-week-old offspring (Extended Data Fig. 10f, g). Additionally, pups with haploinsufficiency or deficiency of maternal TET3 exhibited reduced GCK mRNA and protein levels (Fig. 4d, Extended Data Fig. 10h, i, Supplementary Fig. 1) and glucose intolerance phenotype (Fig. 4e, Extended Data Fig. 10j, k). Therefore, TET3 haploinsufficiency or deficiency in oocytes impedes zygotic reprogramming at the *Gck* promoter, driving the epigenetic inheritance of diabetes susceptibility.

To interrogate whether exogenous TET3 enzyme could alleviate the maternal effects on offspring, HG MII oocytes were injected with wild-type *Tet3* mRNA or a mutant mRNA encoding a catalytically inactive form (hereafter TET3-mut) before IVF (Extended Data Fig. 11a). Immunofluorescence assay revealed substantially increased 5hmC signals in the male pronuclei of zygotes derived from oocytes injected with wild-type but not mutant *Tet3* (Extended Data Fig. 11b). Notably, the supplementation of *Tet3* mRNA in HG MII oocytes resulted in a less methylated state as exemplified by

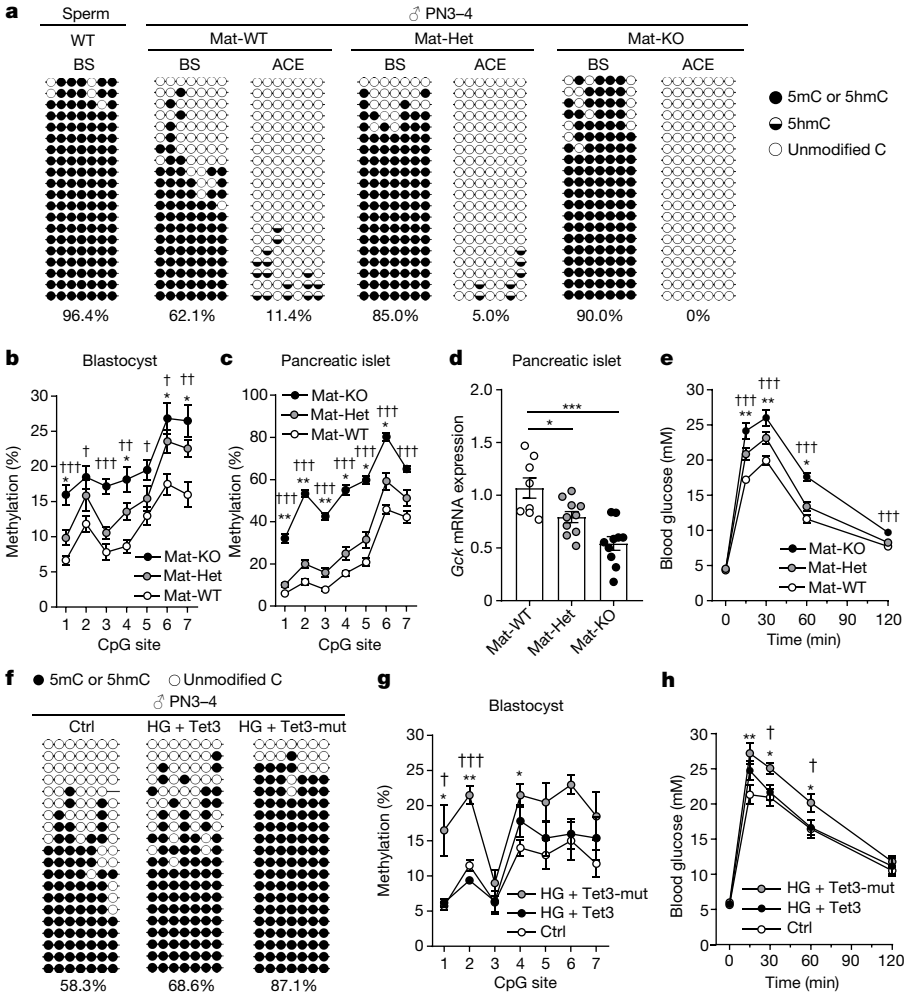

Fig. 4 | Maternal *Tet3* deficiency in mouse oocytes leads to impaired demethylation at the *Gck* promoter and glucose intolerance in offspring, and exogenous *Tet3* expression in HG oocytes reverses the maternal effect. **a**–**e**, Mat-WT, Mat-Het and Mat-KO denote the oocyte-specific *Tet3* genotype of dams from which the analysed embryos or offspring were derived. **a**, Bisulfite and ACE sequencing analyses of the *Gck* promoter in sperm and male pronuclei isolated from aphidicolin-treated PN3–4 zygotes. **b**, **c**, Pyrosequencing analysis of the *Gck* promoter in blastocysts (**b**) and E18.5 pancreatic islets (**c**). $n = 6$ (Mat-WT), 7 (Mat-Het) and 6 (Mat-KO) (with 5 blastocysts pooled for each replicate) for blastocysts; $n = 9$ (Mat-WT), 8 (Mat-Het) and 8 (Mat-KO) mice for fetal islets. **d**, *Gck* mRNA expression in 3-week-old male pancreatic islets. $n = 8$ (Mat-WT), 10 (Mat-Het) and 8 (Mat-KO) mice. **e**, GTT of male offspring at 16 weeks of age. $n = 15$ (Mat-WT), 13 (Mat-Het) and 14 (Mat-KO). For Mat-Het offspring in **c**–**e**, only $Tet3^{+/+}$ pups were used. *Comparison of Mat-Het and Mat-WT; †comparison of Mat-KO and Mat-WT. **f**–**h**, HG + *Tet3* and HG + *Tet3*-mut denote the analysed embryos or offspring from HG MII oocytes injected with wild-type *Tet3* mRNA or inactive *Tet3* mutant mRNA. Embryos or offspring from MII oocytes, derived from non-hyperglycaemic mice and injected with H_2O were used as the control group. **f**, Bisulfite sequencing analysis of the *Gck* promoter in male pronuclei isolated from aphidicolin-treated PN3–4 zygotes. **g**, Pyrosequencing analysis of the *Gck* promoter methylation in mouse blastocysts. $n = 4$ (Ctrl), 5 (HG + *Tet3*), 4 (HG + *Tet3*-mut) with 5 blastocysts pooled for each replicate. **h**, GTT for male offspring at one year of age with natural ageing. $n = 11$ (Ctrl), 10 (HG + *Tet3*), 10 (HG + *Tet3*-mut). *Comparison of HG + *Tet3*-mut and Ctrl; †comparison of HG + *Tet3* and HG + *Tet3*-mut. Data are mean ± s.e.m.; two-tailed *P*-values by unpaired Student's *t*-test with Mat-WT (**b**–**d**) or HG + *Tet3*-mut (**g**), and one-way repeated-measurements ANOVA followed by post hoc unpaired *t*-test with Mat-WT (**e**) or with HG + *Tet3*-mut (**h**). $^{*}P < 0.05$, $^{**}P < 0.01$, $^{***}P < 0.001$, $^{\dagger}P < 0.05$, $^{\dagger\dagger}P < 0.01$ and $^{\dagger\dagger\dagger}P < 0.001$. Statistical details are in Supplementary Table 5.

the *Gck* promoter in male pronuclei and blastocyst embryos (Fig. 4f–g, Extended Data Fig. 11c–g). Consistently, the resultant offspring showed increased expression of GCK at both mRNA and protein levels (Extended Data Fig. 11h, i, Supplementary Fig. 1) and became more tolerant to glucose administration, as indicated by decreased blood glucose area under the curve (AUC) (Fig. 4h, Extended Data Fig. 11j–m). These experiments suggest that the glucose intolerance in offspring induced by maternal hyperglycaemia is directly linked to oocyte TET3 insufficiency.

Discussion

Previous studies have established the transmission of traits acquired by environmental exposure, including HFD, via gametes to offspring and have proposed the possibility of persistent alteration of the genomic methylome as one of the epigenetic variations carried in gametes[16,17]. Our findings demonstrate that a maternal environmental effect on offspring occurs by affecting the level of oocyte TET3, which in turn impinges on zygotic paternal genome reprogramming. Impaired DNA demethylation and epigenetic inheritance affect the expression of a subset of paternally hypermethylated genes involved in insulin secretion, including *Gck*—which is critical for glucose metabolism—thus sensitizing offspring to glucose intolerance. Moreover, injection of mRNA encoding catalytically active TET3—but not the inactive form—in MII oocytes from hyperglycaemic mothers is sufficient to rescue the maternal effect on glucose intolerance in offspring. These data do not support the notion that epigenome alterations in mature oocytes upon

exposure to maternal hyperglycaemia make a critical contribution to the susceptibility of the offspring. Instead, they suggest that *Tet3* transcript levels are vulnerable during oocyte growth and maturation, and that the reduction in oocyte TET3 renders the offspring more susceptible to metabolic disease.

Tet-mediated DNA demethylation in response to high glucose varies among different tissues and species in a context-dependent manner[43–47]. We have revealed a critical window in oocyte growth and maturation that is vulnerable to metabolic perturbation by high glucose. Further work is needed to investigate how Tet function might be disturbed during germ cell development by various environmental challenges, rendering offspring susceptible to diseases. Importantly, TET3-mediated epigenetic inheritance of risk predisposition is not restricted to the mouse model, but also appears relevant to oocytes from women with diabetes mellitus. Our findings call for new guidance on pre-conception care for early prevention, regular screening and glucose control for diabetes among women of reproductive age to protect against disease in the subsequent generation.

Online content

Any methods, additional references, Nature Research reporting summaries, source data, extended data, supplementary information, acknowledgements, peer review information; details of author contributions and competing interests; and statements of data and code availability are available at https://doi.org/10.1038/s41586-022-04756-4.

1. International Diabetes Federation. IDF Diabetes Atlas, 10th edn. Brussels, Belgium: International Diabetes Federation, 2021.
2. Pettitt, D. J., Baird, H. R., Aleck, K. A., Bennett, P. H. & Knowler, W. C. Excessive Obesity in Offspring of Pima Indian Women with Diabetes during Pregnancy. *New Engl. J. Med.* **308**, 242–245 (1983).
3. Hjort, L. et al. Diabetes in pregnancy and epigenetic mechanisms-how the first 9 months from conception might affect the child's epigenome and later risk of disease. *Lancet Diabetes Endocrinol* **7**, 796–806 (2019).
4. Gu, T. P. et al. The role of Tet3 DNA dioxygenase in epigenetic reprogramming by oocytes. *Nature* **477**, 606–610 (2011).
5. Zimmet, P. Z., Magliano, D. J., Herman, W. H. & Shaw, J. E. Diabetes: a 21st century challenge. *Lancet Diabetes & Endocrinology* **2**, 56–64 (2014).
6. Clausen, T. D. et al. High Prevalence of Type 2 Diabetes and Pre-Diabetes in Adult Offspring of Women With Gestational Diabetes Mellitus or Type 1 Diabetes The role of intrauterine hyperglycemia. *Diabetes Care* **31**, 340–346 (2008).
7. Tam, W. H. et al. In Utero Exposure to Maternal Hyperglycemia Increases Childhood Cardiometabolic Risk in Offspring. *Diabetes Care* **40**, 679 (2017).
8. Lowe, W. L. et al. Hyperglycemia and Adverse Pregnancy Outcome Follow-up Study (HAPO FUS): Maternal Gestational Diabetes Mellitus and Childhood Glucose Metabolism. *Diabetes Care* **42**, 372–380 (2019).
9. Watson, E. D. & Rakoczy, J. Fat eggs shape offspring health. *Nat. Genet.* **48**, 478–479 (2016).
10. Sales, V. M., Ferguson-Smith, A. C. & Patti, M. E. Epigenetic Mechanisms of Transmission of Metabolic Disease across Generations. *Cell Metab* **25**, 559–571 (2017).
11. Harris, J. E. et al. Exercise-induced 3′-sialyllactose in breast milk is a critical mediator to improve metabolic health and cardiac function in mouse offspring. *Nature Metabolism* **2**, 678–687 (2020).
12. Godfrey, K. M., Gluckman, P. D. & Hanson, M. A. Developmental origins of metabolic disease: life course and intergenerational perspectives. *Trends Endocrinol. Metab.* **21**, 199–205 (2010).
13. Skinner, M. K., Manikkam, M. & Guerrero-Bosagna, C. Epigenetic transgenerational actions of environmental factors in disease etiology. *Trends Endocrinol. Metab.* **21**, 214–222 (2010).
14. Rando, O. J. & Simmons, R. A. I'm eating for two: parental dietary effects on offspring metabolism. *Cell* **161**, 93–105 (2015).
15. Boskovic, A. & Rando, O. J. in *Annual Review of Genetics, Vol 52 Vol. 52 Annual Review of Genetics* (ed N. M. Bonini) 21-41 (2018).
16. Ge, Z. J. et al. DNA methylation in oocytes and liver of female mice and their offspring: effects of high-fat-diet-induced obesity. *Environ. Health Perspect.* **122**, 159–164 (2014).
17. Huypens, P. et al. Epigenetic germline inheritance of diet-induced obesity and insulin resistance. *Nat. Genet.* **48**, 497–499 (2016).
18. Daxinger, L. & Whitelaw, E. Understanding transgenerational epigenetic inheritance via the gametes in mammals. *Nat. Rev. Genet.* **13**, 153–162 (2012).
19. Chen, Q., Yan, W. & Duan, E. Epigenetic inheritance of acquired traits through sperm RNAs and sperm RNA modifications. *Nat. Rev. Genet.* **17**, 733–743 (2016).
20. Mauvais-Jarvis, F. Estrogen and androgen receptors: regulators of fuel homeostasis and emerging targets for diabetes and obesity. *Trends Endocrinol. Metab.* **22**, 24–33 (2011).
21. Muoio, D. M. & Newgard, C. B. Molecular and metabolic mechanisms of insulin resistance and β-cell failure in type 2 diabetes. *Nat. Rev. Mol. Cell Biol.* **9**, 193–205 (2008).
22. Kleinert, M. et al. Animal models of obesity and diabetes mellitus. *Nat. Rev. Endocrinol.* **14**, 140–162 (2018).
23. Reik, W., Dean, W. & Walter, J. Epigenetic reprogramming in mammalian development. *Science* **293**, 1089–1093 (2001).
24. Sharma, U. & Rando, O. J. Metabolic Inputs into the Epigenome. *Cell Metabolism* **25**, 544–558 (2017).
25. Cavalli, G. & Heard, E. Advances in epigenetics link genetics to the environment and disease. *Nature* **571**, 489–499 (2019).
26. Wossidlo, M. et al. 5-Hydroxymethylcytosine in the mammalian zygote is linked with epigenetic reprogramming. *Nat. Commun.* **2**, 241 (2011).
27. Iqbal, K., Jin, S.-G., Pfeifer, G. P. & Szabó, P. E. Reprogramming of the paternal genome upon fertilization involves genome-wide oxidation of 5-methylcytosine. *Proc. Natl Acad. Sci.* **108**, 3642–3647 (2011).
28. Tan, L. & Shi, Y. G. Tet family proteins and 5-hydroxymethylcytosine in development and disease. *Development* **139**, 1895 (2012).
29. Wang, Q., Chi, M. M., Schedl, T. & Moley, K. H. An intercellular pathway for glucose transport into mouse oocytes. *Am J Physiol Endocrinol Metab* **302**, E1511–E1518 (2012).
30. Spruijt, C. G. & Vermeulen, M. DNA methylation: old dog, new tricks? *Nat. Struct. Mol. Biol.* **21**, 949–954 (2014).
31. Boyes, J. & Bird, A. DNA methylation inhibits transcription indirectly via a methyl-CpG binding protein. *Cell* **64**, 1123–1134 (1991).
32. Iynedjian, P. B. Molecular physiology of mammalian glucokinase. *Cell. Mol. Life Sci.* **66**, 27–42 (2009).
33. Efrat, S. et al. Ribozyme-mediated attenuation of pancreatic β-cell glucokinase expression in transgenic mice results in impaired glucose-induced insulin secretion. *Proc Natl Acad Sci U S A* **91**, 2051–2055 (1994).
34. Grupe, A. et al. Transgenic knockouts reveal a critical requirement for pancreatic β cell glucokinase in maintaining glucose homeostasis. *Cell* **83**, 69–78 (1995).
35. Terauchi, Y. et al. Pancreatic β-cell-specific targeted disruption of glucokinase gene. Diabetes mellitus due to defective insulin secretion to glucose. *J. Biol. Chem.* **270**, 30253–30256 (1995).
36. Shen, J. & Zhu, B. Integrated analysis of the gene expression profile and DNA methylation profile of obese patients with type 2 diabetes. *Molecular medicine reports* **17**, 7636–7644 (2018).
37. Joglekar, M. V. et al. Expression of miR-206 in human islets and its role in glucokinase regulation. *American journal of physiology. Endocrinology and metabolism* **315**, E634–e637 (2018).
38. Cauchi, S. et al. European genetic variants associated with type 2 diabetes in North African Arabs. *Diabetes & metabolism* **38**, 316–323 (2012).
39. Bonnefond, A. et al. Pathogenic variants in actionable MODY genes are associated with type 2 diabetes. *Nature Metabolism* **2**, 1126–1134 (2020).
40. Terauchi, Y. et al. Glucokinase and IRS-2 are required for compensatory β cell hyperplasia in response to high-fat diet-induced insulin resistance. *J. Clin. Invest.* **117**, 246–257 (2007).
41. Lu, B. et al. Impaired β-cell glucokinase as an underlying mechanism in diet-induced diabetes. *Dis. Models Mech.* **11**, dmm033316 (2018).
42. Tang, L. et al. Elevated CpG island methylation of GCK gene predicts the risk of type 2 diabetes in Chinese males. *Gene* **547**, 329–333 (2014).
43. Dhliwayo, N., Sarras, M. P. Jr, Luczkowski, E., Mason, S. M. & Intine, R. V. Parp inhibition prevents ten-eleven translocase enzyme activation and hyperglycemia-induced DNA demethylation. *Diabetes* **63**, 3069–3076 (2014).
44. Wu, D. et al. Glucose-regulated phosphorylation of TET2 by AMPK reveals a pathway linking diabetes to cancer. *Nature* **559**, 637–641 (2018).
45. Zhang, Q. et al. Differential regulation of the ten-eleven translocation (TET) family of dioxygenases by O-linked β-N-acetylglucosamine transferase (OGT). *J. Biol. Chem.* **289**, 5986–5996 (2014).
46. Yuan, E.-F. et al. Hyperglycemia affects global 5-methylcytosine and 5-hydroxymethylcytosine in blood genomic DNA through upregulation of SIRT6 and TETs. *Clinical Epigenetics* **11**, 63 (2019).
47. Pinzon-Cortes, J. A. et al. Effect of diabetes status and hyperglycemia on global DNA methylation and hydroxymethylation. *Endocr Connect* **6**, 708–725 (2017).

Methods

Animal use and care

The animal study protocols were approved by the Animal Care and Use Committee of Zhejiang University and CAS Center for Excellence in Molecular Cell Science, Shanghai Institute of Biochemistry and Cell Biology, Chinese Academy of Sciences, China. All animal experiments were carried out according to the rules and guidelines of the local animal ethics committee. Mice and rats were housed in a 12-h light-dark cycle in climate-controlled, pathogen-free barrier facilities with humidity range of 40%–70% and temperature range of 20–26 °C in a climate-controlled clean room on a 12-h/12-h light/dark cycle. Mice and rats had ad libitum access to water and food.

HG mouse model

At the age of 7–8 weeks, fasted virgin female C57BL/6N mice were randomly divided into two groups and intraperitoneally injected with STZ (Sigma) at a dose of 150 mg kg^{-1} or the same volume of citrate buffer[1–3]. Mice that received citrate buffer (vehicle) served as controls, and those that received STZ injection and had nonfasting blood glucose concentrations above 16.7 mM (300 mg dl^{-1}) on the 30th day of IVF were defined as HG mothers. Blood glucose concentrations from the tail vein were measured using a glucometer (Roche Diagnostics Accu-Chek). For *Tet3* transcript level measurements, female mice that received STZ injection were further divided into three subgroups according to the nonfasting glucose level on the day of oocyte retrieval: blood glucose above 33.3 mM (600 mg dl^{-1}) was defined as severe, between 16.7 and 33.3 mM (300–600 mg dl^{-1}) was defined as moderate, and below 8.3 mM (150 mg dl^{-1}) was defined as normal (Extended Data Fig. 6a).

T2DM mouse model

T2DM mice were modelled as described[4]. Female C57BL/6J mice aged 4 weeks were fed with a high-fat diet (HFD; 60% of calories from fat; Research Diets, D12492) or a normal chow diet. After 4 weeks, HFD mice were injected intraperitoneally with a single dose of STZ (100 mg kg^{-1}). Mice fed with a chow diet received citrate buffer alone and were processed in parallel with the diabetic mice. All mice were maintained on their respective diets for another 8 weeks until the end of the study.

IVF, embryo transfer and offspring generation

Germline-dependent inheritance experiments were conducted as previously described[5]. Female oocyte donors were euthanized for production of the offspring cohorts. Offspring cohorts for the control and HG groups were generated on the same day. IVF assays were performed following a standard protocol[6]. In brief, sperm were obtained from the dissected epididymis of one sperm donor for all parallel groups and capacitated for 1 h in HTF medium (Merck Millipore). The cumulus–oocyte complexes (COCs) were isolated from oviducts 14–16 h after human chorionic gonadotropin (hCG) injection and then incubated with sperm in HTF medium at 37 °C with 5% CO_2. The zygotes were cultured until 2-cell embryo formation. The well-developed 2-cell embryos were selected and transferred into the oviducts of ICR foster mothers.

Litter sizes of 6–12 was used for the experiments and then randomly reduced to no more than 8 to ensure equal access to breast milk for the pups. The offspring identities were marked by toe clipping on day 7, and the weaned pups from different groups were redistributed ad libitum according to sex. Pups from different groups were cohabited to maintain identical environments and reduce other variables (microbiota, circadian rhythm, and so on).

Glucose metabolism measurements

The metabolic measurements were conducted in a blinded manner. The offspring from different groups were cohabited and then remarked temporarily on the tail with a felt tip marker. Experimenters were blinded to the mouse identities marked by permanent toe clipping, and the phenotyping procedures were carried out by the experimenters based on the temporary markers. The mice were handled daily for a week before the test to allow them to get used to the handling to minimize stress. For HFD challenge, both male and female offspring were fed with a high-fat diet (HFD; 60% of calories from fat) from 3 weeks of age onwards. Glucose metabolism measurements were performed on offspring according to a previous report[7].

For the GTTs, mice were fasted overnight and injected intraperitoneally with D-glucose (Sigma) saline water (2 g kg^{-1} body weight). Blood glucose concentration was measured via tail vein blood in the fasted state and at 15, 30, 60 and 120 min after glucose administration using the glucometer (AccuCheck, Roche). AUCs were calculated as an index of whole glucose excursion in the blood after glucose loading, which has been widely used for evaluating the efficacy of insulin for the maintenance of glucose homeostasis.

Insulin tolerance tests (ITTs) were conducted after 4 h of fasting, and blood glucose levels were measured before and 15, 30, 60 and 120 min after the intraperitoneal injection of insulin (Novolin R, Novo Nordisk; 0.75 U kg^{-1} body weight). Data are presented as the percentages of basal glucose level.

Isolation of pancreatic islets

Adult and E18.5 fetal pancreases were dissected and digested according to our previous publication, with minor modifications[8]. For adult mice, the animals were killed, and the gall bladder area was exposed. After clamping at the confluence of the common bile duct and duodenum, the bile duct was perfused with collagenase IV (2 mg ml^{-1}; Worthington), and the pancreas was distended. The pancreas was then excised and shaken at 37 °C for 28 min. After washing and centrifugation, adult islets were handpicked under a stereomicroscope. For E18.5 fetal mice, the pancreases were dissected and digested directly in collagenase IV under the same conditions, washed, centrifuged and then recovered in RPMI 1640 medium with 5 mM glucose for 6 h in the incubator and handpicked under a stereomicroscope.

Insulin secretion function test

For the in vivo test, mice that had fasted overnight were injected with D-glucose saline water (2 g kg^{-1} body weight), and blood samples were collected through the orbital vein before and 30 min after glucose load. We calculated the insulinogenic index by dividing the increment in serum insulin (ΔIns_{0-30}; in μU ml^{-1}) by the increment in plasma glucose (ΔGlu_{0-30}; in mM) during the 0 to 30 min time periods of the intraperitoneal glucose tolerance test (ipGTT). Blood glucose levels were determined using a glucometer. Serum insulin was measured by radioimmunoassay (iodine (^{125}I) radioimmunoassay kit; BNIBT).

For the in vitro test, the isolated islets were incubated for 4 h in RPMI 1640 medium with 5 mM glucose for recovery, distributed to ten size-matched islets for each well and incubated for 1 h in RPMI 1640 medium with no glucose for starvation. In Fig. 1d, for baseline secretion, islets were rinsed and cultured in 5 mM D-glucose Krebs–Ringer bicarbonate buffer (KRBB) in an incubator for 1 h. For stimulated secretion, islets were again rinsed and cultured in 25 mM D-glucose KRBB for 1 h. After islets were removed, supernatants were mixed and collected for insulin content measurements by ELISA. The stimulation index was calculated as the insulin content secreted in 25 mM divided by that in 5 mM. Two batch replicates were performed to obtain an average value for each mouse. Insulin contents were measured by ultrasensitive ELISA kits according to the instructions from the manufacturer (CrystalChem).

Measurement of pancreatic insulin content

To measure pancreatic insulin content, the whole pancreas was isolated, homogenized in acid alcohol, and extracted overnight at 4 °C. The extract was centrifuged to remove unhomogenized tissue and neutralized with 1 M Tris at pH 7.5. Protein concentration was examined with a BCA Protein Assay Kit (Thermo Scientific). The supernatant was used

for the measurement of insulin content by using ultrasensitive Mouse Insulin ELISA kit (Crystal Chem).

Histological and morphometric analysis of pancreatic islets

Animals were fasted overnight before dissection. For histological studies, pancreas samples were rinsed in cold PBS and fixed overnight in 4% paraformaldehyde. The pancreases were then processed and embedded in paraffin, and consecutive sections were obtained. The largest cross-section of each pancreas was taken to perform insulin immunohistochemistry (IHC) to mark pancreatic islets and perform insulin and glucagon immunofluorescence to present the ratio of α- or β-cell. The tissue slices were de-paraffinized in xylene and rehydrated in ethanol. Sections were stained with anti-insulin (CST 3014, 1:500 for immunofluorescence, 1:400 for IHC) and anti-glucagon (R&D systems MAB1249, 1:500) and were revealed using fluorescent-conjugated secondary antibodies (647-conjugated, Invitrogen A21247, 1:800; AlexaFluor 488-conjugated, Abcam 150077, 1:500) for multiple labelling or DAB chromogenic agent kit (Servicebio). Images were captured using Olympus BX51 microscope and Olympus FV3000 confocal laser scanning microscope.

For islet parameter analysis, paraffin-embedded pancreas sections (4 μm) were stained with haematoxylin and eosin (H&E). The cross-sectional areas of islet from H&E-stained sections were measured from at least two slices per individual pancreas from the largest cross-sections, evenly sectioned and separated by 100 μm. Images were scanned using a Pannoramic DESK. Images of islets were traced manually and analysed using CaseViewer software.

Mouse oocyte and embryo collection

To obtain oocytes and embryos, MII oocytes were denuded with 0.5 mg ml^{-1} hyaluronidase (Sigma), and zona pellucida were removed with Tyrode's solution (Sigma), rinsed and stored in DPBS buffer supplemented with 0.2% BSA. The GV oocytes were obtained from ovarian follicles in M2 medium (Sigma) with 200 μM 3-isobutyl-1-methylxanthine (IBMX) (Sigma) 48 h after pregnant mare serum gonadotropin (PMSG) priming. The PN3–4 zygotes were selected from IVF assays 7–8 h after fertilization. To obtain blastocysts, IVF-derived 2-cell embryos were cultured in KSOM medium (Merck Millipore) for an additional 48–72 h in the incubator. Only the oocytes and embryos with good morphology and appropriate developmental speed were included for biochemical evaluation.

DNA library preparation for RNA-seq

For MII oocytes, every 10 MII oocytes from a single mouse were pooled for one group. All groups were preamplified to obtain cDNA by the SMART-Seq2 protocol[48]. cDNA was quantified by Qubit 3.0 (Thermo Fisher Scientific) and 1 ng cDNA was used for DNA library construction with TruePrep DNA Library Prep Kit V2 for Illumina (Vazyme) following the manufacturer's instructions.

RNA-seq data analysis

First, the raw pair-end RNA-seq FASTQ data were trimmed to remove low-quality bases and adaptor sequences by Trim Galore (v0.5.0) with default settings. Then the clean RNA-seq FASTQ data were mapped to mouse reference genome mm10 using hisat2 (v2.1.0) with default parameters. Differentially expressed gene analysis was performed by using DESeq2 package with the raw count. Only genes with adjusted *P*-value (attained by the Wald test and corrected for multiple testing using the Benjamini–Hochberg method by default) less than 0.05 and at least 1.5-fold change were considered to be differentially expressed. To perform KEGG analysis, the DEGs were submitted to the DAVID 6.8 website, and Fisher's Exact test was used to measure the gene enrichment in annotation terms.

Ethics statement

This study was approved by the ethics committees of the International Peace Maternity and Child Health Hospital, School of Medicine, Shanghai Jiao Tong University (2019-02), Sir Run Run Shaw Hospital, School of Medicine, Zhejiang University (20190617-3) and Women's Hospital, School of Medicine, Zhejiang University (20190064). All the experiments, the composition of the ethics committees and the informed consent process complied with International Society for Stem Cell Research (ISSCR) Guidelines for Stem Cell Research and Clinical Translation (2016), Guidelines for Human Assisted Reproductive Technology (2003) and the Ethical Principles of the Human Assisted Reproductive Technology and the Human Sperm Bank (2003) issued by the Ministry of Health of People's Republic of China, and the Helsinki declaration (2013). All the medicine ethics committees involved are composed of members including qualified scientists, ethicists, legal and regulatory experts and community members. All human oocytes used involved in the study were immature and collected in IVF or intracytoplasmic sperm injection (ICSI) cycles. For IVM experiments, immature oocytes were cultured under various glucose concentrations until MII stage and were not used for fertilization or forming embryos. All the donated blastocysts were from patients who underwent pre-implantation genetic diagnosis/screening (PGD/PGS) and were identified with genetic or chromosomal abnormalities thus unable to develop healthy offspring. All donor couples signed informed consents for voluntary donations of immature oocytes and genetic or chromosomal abnormal blastocytes. In the process, couples were informed that their donation would not affect their assisted reproductive technology (ART) treatment. No financial inducements were offered for the donations.

Sample collection from patients

All the human samples in the current study were follicular fluid, oocytes and blastocysts from the patients who underwent ART. All the oocytes involved in the current study were immature and unavailable for ICSI, and blastocysts with genetic or chromosomal abnormalities were from patients who underwent PGD/PGS. Among the patients underwent ART, the diabetic females (with fasting blood glucose ≥7.0 mM or 2 h glucose in GTT ≥11.1 mM) were in the diabetes group, and those non-diabetic females with normal glucose levels and without a history of diabetes were in the control group. For oocytes collection, each diabetic patient was paired with two control patients. The paired controls were matched with diabetic patients according to the following variables: age (within 4 years) and superovulation protocol (GnRH-agonist regimen or GnRH-antagonist regimen). For blastocysts collection, all the involved males displayed normal semen analysis and fasting glucose test results. The follicular fluid from nondiabetic and diabetic women was obtained during the oocyte retrieval process. The glucose concentrations in all samples were measured with a glucometer. For immature oocytes collected for IVM, all the women were infertile owing to nonovarian reasons, younger than 35 years old, displayed no endocrine or metabolic disorders, and had no chromosome abnormalities. Detailed information of the patients is listed in Supplementary Table 2.

In vitro maturation of human oocytes

Immature oocytes were denuded with hyaluronidase (Irvine Scientific) on the day of ovum retrieval and collected, and then randomly distributed in G-IVF medium (Vitrolife) supplemented with various D-glucose concentrations and cultured at 37 °C with 6% CO_2. Only competent MII oocytes were collected for further analysis.

In vitro culture of human blastocysts

Zygotes (fertilized by ICSI) were cultured in G1-plus medium (Vitrolife) in 20 μl droplets covered with mineral oil (Sage) until day 3. Then, the embryos were cultured in G2-plus medium (Vitrolife) in 20 μl droplets until day 5 or 6. Blastocysts were vitrified at 30 min after biopsy using vitrification solution (Kitazato). Blastocysts with genetic or chromosomal abnormalities for bisulfite sequencing were thawed following standard clinical protocols by using thaw solution (Kitazato) and

transferred to G2-plus culture medium for 2 h to evaluate their survival. Blastocysts with a smooth trophectoderm, clearly visible blastocyst cavity and well-developed inner cell mass were used in this study.

Follicular fluid collection and glucose concentration measurements in rats

As the mouse model provided insufficient volume of follicular fluid, a hyperglycaemic rat model was established in an identical fashion as the HG mouse model by injecting 60 mg kg^{-1} STZ; these rats had a nonfasting glucose level above 16.7 mM (300 mg dl^{-1}). The follicular fluid was collected from ovarian antral follicles after PMSG priming as described[49]. In brief, rat follicular fluid was obtained using a fine glass capillary tube under ice-cold mineral oil by capillary action.

In vitro maturation of mouse oocytes

For mice, denuded GV oocytes were collected from the ovarian follicles of mice after PMSG priming in M2 with 200 μM IBMX. After being washed twice, GV oocytes were randomly distributed and incubated in M16 medium with various glucose concentrations at 37 °C with 5% CO_2. After 12 h, the competent MII oocytes (with the first polar body extruded) after zona pellucida removal were rinsed in DPBS and stored at −80 °C.

In vitro growth

We mainly followed the published protocols[50]. To collect mouse follicles for in vitro culture, ovaries were obtained from 12-day-old females and transformed into M2 medium. Puncture them using a 30-gauge needle to release follicles. Select follicles with diameters around 120 μm and cultured individually in 20 μl culture medium: α-MEM (Gibco) supplemented with 5% of fetal bovine serum, 1× ITS liquid media supplement (Sigma), 1× nucleosides (Millipore), 1× penicillin-streptomycin and 100 mIU ml^{-1} PMSG. Follicles were cultured in the incubator at 37 °C and 5% CO_2 in air and 10 μl of culture medium was added to each follicle after 24 h. Half of the medium was changed every other day. After 12 days, 70–80% of oocytes reached the fully grown GV stage.

RNA extraction, reverse transcription and quantitative real-time PCR

For pancreatic islets, total RNA was extracted using an RNeasy Micro Kit (Qiagen) according to the instruction manual. cDNA was synthesized using a PrimeScript RT reagent Kit (Takara) when *Actb* and *Hprt* were used as internal controls for normalization. PrimeScript RT reagent was used with the gDNA Eraser Kit (Takara) when 18S rRNA was used for normalization. To analyse small amounts of oocytes or blastocysts, RNA extraction, PCR with reverse transcription (RT–PCR) and cDNA amplification were carried out following the Smart-seq2 protocol[48]. To measure gene expression, real-time quantitative PCR was performed on a Roche LightCycler 480 with SYBR Premix Ex Taq (Tli RNaseH Plus, Takara). Unless otherwise stated, the gene expression levels were normalized to those of *Actb* or *ACTB* and further confirmed by normalization to those of *Hprt* or *HPRT1*. All primer sequences are shown in Supplementary Table 4.

Immunofluorescence of zygotes

Zygotes were fixed with 4% paraformaldehyde for 15 min, permeated with 0.2% Triton X-100 for 20 min, denatured in 4 N HCl solution for 10 min and neutralized in Tris-HCl (pH 8.0) for 10 min for 5mC and 5hmC staining but without HCl denaturation for TET3 and DAPI staining. The zygotes were then blocked in 5% BSA solution diluted in PBS containing 0.2% Triton X-100 for 1 h. Samples were stained overnight at 4 °C with the primary antibodies (anti-TET3: Active motif 61744, 1:300; anti-5mC: Calbiochem NA81, 1:1,000; anti-5hmC: active motif 39770, 1:500) and for 1 h at room temperature with the secondary antibodies (594-conjugated, Jackson ImmunoResearch 711-585-152, 1:800; 488-conjugated, Jackson ImmunoResearch 715-545-150, 1:800). Samples were mounted onto slides with antifade medium containing DAPI (Abcam) and examined under Olympus Fluoview FV1000 or Zeiss LSM880 with Ariyscan laser-scanning confocal microscope. *Z*-stack mode was used to merge 7–8 layers (every 0.1 μm) by FV21S-SW Viewer or ZEN 2.3 Lite to calculate intensity using ImageJ 1.52j software (National Institutes of Health).

Intracytoplasmic sperm injection

Sperm of CAST/EiJ male mice were collected from cauda epididymis and incubated in HTF medium for 10–15 min at 37 °C under 5% CO_2 before use. Control and HG MII oocytes were isolated from superovulated female mice 14–15 h after injection with hCG. Oocytes were operated in a drop of M2 medium containing 5 μg ml^{-1} cytochalasin B, and single spermatozoa were injected into oocyte cytoplasm with a Piezo-drill micromanipulator. After injection the embryos were cultured in KSOM medium. Two-cell stage embryos were transferred into oviducts of pseudopregnant ICR females at 0.5 days post-conception (dpc) to generate offspring, and pancreatic islets were collected for postbisulfite adaptor tagging (PBAT) library preparation (E18.5 fetuses).

PBAT library preparation

Pancreatic islets of three fetuses from one pregnant mouse were pooled as one sample for library building, and both the control and HG groups had three replicates from three dams. All groups were used to construct the PBAT library using a previously described protocol[51] with slight modifications. The final quality-ensured libraries were pooled and sequenced on the Illumina HiSeq X ten sequencer for 150 bp paired-end sequencing.

PBAT data analysis

By using Trim Galore (v0.5.0), raw pair-end FASTQ reads were trimmed to remove low quality bases and adaptor sequences. The remaining clean reads were mapped to mouse reference genome mm10 with single-end and non-directional mapping parameters by using BS-seeker2[52] (v2.1.8). Duplicated reads were removed using Picard (v2.21.2) for the subsequent analysis. Bisulfite conversion rate was estimated by the Lambda genome, which was built as the extra chromosome. Only samples with at least 97.5% bisulfite conversion rate were kept for DNA methylation analysis.

CGmapTools (v0.1.2)[53] was used for DNA methylation downstream analysis following BS-Seeker2. The single-C files of the replicates were merged together, and only CpG sites with at least 3× coverage were kept for further analysis. The annotated information of exon, intron, intergenic and CpG island (CGI) was downloaded from the UCSC Genome Browser (mm10), and all the repetitive elements were annotated using RepeatMasker (mm10). Promoters were defined as the regions from −2.5 to +2.5 kb of the transcription start site.

DMRs were filtered using dmr command in CGmapTools by the DMR length (less than 1,000 bp), CpG number (at least 5 CpGs in a DMR) and the methylation level difference between control and HG group (at least 20% absolute methylation level difference). Maximal distance between two adjacent cytosines in CpG was 100 bp. *P*-values were calculated by *t*-test according to the DNA methylation levels of all the CpGs in every DMR using dmr command in CGmapTools. To perform KEGG analysis, the genes with promoter DMRs were submitted to the DAVID 6.8 website, and Fisher's exact test was used to measure the gene-enrichment in annotation terms.

Allele-specific methylation analysis

By using SNPsplit[54], we were able to distinguish allele-specific CpG methylation patterns in the hybrid embryos by using the SNPs between CAST/EiJ and C57BL/6J mice. The PBAT data were mapped to mouse reference genome N-masked mm10 with paired end and non-directional mapping parameters by Bismark (v0.19.0). Then, the unmapped reads after the first step alignment were re-aligned to the same reference in

single-end mode. The SNPsplit could split total bam files into C57BL/6J and CAST/EiJ bam files, and bismark_methylation_extractor could call methylation information from bam files. CGmapTools would transfer CpG_report files into CGmap files. The further analysis is similar to PBAT data analysis.

DNA extraction and methylation analysis

For low cell number samples, genomic DNA was extracted with a QIAamp DNA Micro Kit (Qiagen). For sperm, somatic cells were removed by standard cell lysis, and the residual sperm were lysed in 3% sodium dodecyl sulfate (SDS), 0.4 mg ml^{-1} proteinase K, and 44 mM dithiothreitol buffer and incubated overnight at 55 °C. Then, DNA was isolated by ethanol precipitation. Genomic DNA was extracted, and bisulfite was converted with EZ DNA Methylation-Direct Kit (Zymo Research). Bisulfite-treated DNA was amplified with Takara EpiTaq HS (Takara) or PyroMark PCR Kit (Qiagen).

Pyrosequencing

Primers for the pyrosequencing analysis were designed using PyroMark Assay Design software 2.0 (Qiagen). Pyrosequencing was carried out according to the manufacturer's standard protocol on a PyroMark Q24 instrument (Qiagen). The biotinylated PCR products were immobilized with streptavidin-coated Sepharose beads (GE healthcare), purified, denatured, and then annealed to 0.3 μM sequencing primers. Data were analysed using PyroMark Q24 software (Qiagen) to determine the methylation percentage at each CpG site. All primer sequences are shown in Supplementary Table 4.

Bisulfite sequencing

After amplification, PCR products of bisulfite-treated DNA were purified with a Gel Extraction Kit (Qiagen) and cloned into the pMD19-T vector (Takara). Individual clones were sequenced by standard Sanger sequencing (TSINGKE). Data were analysed by the online tool QUMA (http://quma.cdb.riken.jp/).

APOBEC-coupled epigenetic sequencing

ACE sequencing was conducted to determine the 5hmC level following a previous publication[55]. In brief, the genomic DNA mixture was glucosylated using UDP-glucose and T4 β-glucosyltransferase (NEB) at 37 °C for 1 h. One microlitre of DMSO was added, and the sample was denatured at 95 °C for 5 min and snap cooled by transfer to a PCR tube rack preincubated at −80 °C. Human cytosine deaminase APOBEC3A was added to a final concentration of 5 μM in a total volume of 10 μl. The deamination reactions were incubated under linear ramping temperature conditions from 4–50 °C over 2 h. PCR amplification and sequencing were carried out as described above.

Isolation of male and female pronuclei

IVF-derived zygotes were treated with replication inhibitor aphidicolin (3 μg ml^{-1}) at 4 h after fertilization[56,57]. Male pronuclei and female pronuclei, which were distinguished on the basis of their size and distance from polar bodies[58], were collected from zygotes of PN3–4 stages by breaking the zona using a piezo drive (Prime Tech) and aspirating using a micromanipulator. More than 200 pronuclei were pooled for the subsequent methylation analysis.

CRISPR–Cas9-mediated editing of *Gck* gene in mouse embryos

We mainly followed the published protocols[59–61]. For microinjection of one-cell embryos, B6D2 F_1 female mice and ICR mice were used as embryo donors and foster mothers, respectively. The embryo-donor female mice were superovulated and mated with wild-type male mice. One-cell-stage embryos were collected from oviducts and injected with *Cas9* mRNA (100 ng μl^{-1}) and single guide RNA (sgRNA) (50 ng μl^{-1}) in RNase-free water. The injected embryos were cultured in KSOM at 37 °C under 5% CO_2 until 2-cell stage and transferred into oviducts of pseudopregnant ICR females at 0.5 dpc. The mice were genotyped as described[62]. The sgRNA sequence and PCR primers for genotyping are listed in Supplementary Table 4. A schematic diagram of the strategy to distinguish the parental DNA methylation pattern of *Gck* promoter is presented in Extended Data Fig. 8e. The bisulfite PCR primers to distinguish allele-specific methylation in this strategy are listed in Supplementary Table 4.

Glucokinase activation

For in vivo GCK activation, glucokinase activator (GKA) Dorzagliatin (HMS-5552, 2mg kg^{-1}) was administered intragastrically (via oral gavage) 15 min before ipGTT assay and control animals received PBS[63–65].

For in vitro GCK activation, islets were pre-incubated in dorzagliatin for 1 h before the GSIS assay[66–68]. In brief, islets from each HG mouse were separated into two groups. Ten islets of each mouse were incubated with 0.5 μM dorzagliatin as the HG + GKA group and another ten were untreated as the HG group. Islets from control mice were left untreated for GSIS assay as the control group.

Tet3 conditional knockout mouse model and offspring generation

Tet3$^{f/f}$ Zp3-Cre mice were generated as described[4]. The offspring were obtained to mimic oocytes with TET3 downregulation from the HG mouse model (Extended Data Fig. 10a, b). In this model, mice were naturally conceived, delivered and nursed. The offspring were also genotyped and cohabited with others of the same sex from three weeks of age.

Protein extraction and immunoblotting

Pancreatic islets were collected from 2–5 mice per sample. Pooled islets were lysed in 50 μl RIPA lysis buffer (50 mM Tris pH 7.6, 150 mM NaCl, 1% NP-40, 0.5% sodium deoxycholate, 0.1% SDS) containing protease inhibitors (protease inhibitor cocktail, Roche) and 0.5 mM PMSF. Tissues were briefly sonicated and protein concentrations were determined by BCA protein assay (Thermo Fisher). Then 6× SDS sample buffer (0.5 M Tris-Cl pH 6.8, 30% (w/v) glycerol, 10% (w/v) SDS, 0.6 M dithiothreitol, 0.012% (w/v) bromophenol blue) was added to a final concentration of 1× and samples were denatured by incubation at 100 °C for 5 min. Lysate samples with equivalent protein levels (50 μg) were loaded on a 10% SDS–PAGE gels and electrophoretically transferred to nitrocellulose membrane (Bio-Rad), followed by primary antibodies against GCK (rabbit polyclonal, 1:200; sc-7908, Santa Cruz) or β-actin (rabbit monoclonal, 1:10,000; AC026, ABclonal) and secondary antibody (peroxidase-conjugated, Jackson ImmunoResearch 111-035-003, 1:10,000). Images were taken by SageCreation and analysed by SageCapture software. β-actin was included as loading control.

In vitro transcription

To prepare mRNAs for microinjection, wild-type *Tet3* or *Tet3* mutant (in which the HKD coding sequence is replaced by the YRA coding sequence) sequence was first cloned into pCAG vector with a sequence encoding a HA tag, and then the sequence of the T7 promoter followed by the desired cDNA was PCR-amplified from the constructed vector. The purified DNA fragments were used as a template for in vitro transcription with mMESSAGE mMACHINE T7 ULTRA Transcription Kit (Invitrogen) according to the manufacturer's instructions. RNA was purified by lithium chloride precipitation. Synthesized RNA was aliquoted and stored at −80 °C until use. GFP-UTR$_{Tet3}$ untailed mRNA was prepared according to the manufacturer's instructions.

Microinjection of oocytes

For GV oocytes microinjection, fully grown GV oocytes were collected in M2 medium with 0.2 mM IBMX to inhibit spontaneous GVBD from superovulated 3-week-old B6D2 F_1 female mice. BFP-polyA, mCherry-UTR$_{Tubb3}$ and GFP-UTR$_{Tet3}$ mRNA were injected into the cytoplasm with equal

mole ratio using a Piezo-drill micromanipulator. Following injection, oocytes were cultured in IVM medium with 0.2 mM IBMX for at least 6 h before subsequent IVM.

For MII oocytes microinjection, wild-type *Tet3*, *Tet3* mutant mRNA (1 μg μl^{-1} in RNase-free water) or H_2O was injected into the cytoplasm using FemtoJet (Eppendorf). After injection, the zona pellucida of each MII oocyte was punched to make a small hole using Piezo-drill micromanipulator. Then MII oocytes were washed and cultured in KSOM for at least 3 h before subsequent IVF.

Reporting summary

Further information on research design is available in the Nature Research Reporting Summary linked to this paper.

Data availability

All the sequencing data can be viewed in NODE under accession OEP002503. All other data are available from the corresponding authors on reasonable request. Statistical details are in Supplementary Table 5. Full immunoblots are provided as Supplementary Fig. 1. Source data are provided with this paper.

48. Picelli, S. et al. Full-length RNA-seq from single cells using Smart-seq2. *Nat. Protoc.* **9**, 171–181 (2014).
49. Harris, S. E., Gopichandran, N., Picton, H. M., Leese, H. J. & Orsi, N. M. Nutrient concentrations in murine follicular fluid and the female reproductive tract. *Theriogenology* **64**, 992–1006 (2005).
50. Gu, C., Liu, S., Wu, Q., Zhang, L. & Guo, F. Integrative single-cell analysis of transcriptome, DNA methylome and chromatin accessibility in mouse oocytes. *Cell Res* **29**, 110–123 (2019).
51. Smallwood, S. A. et al. Single-cell genome-wide bisulfite sequencing for assessing epigenetic heterogeneity. *Nat. Methods* **11**, 817–820 (2014).
52. Guo, W. et al. BS-Seeker2: a versatile aligning pipeline for bisulfite sequencing data. *BMC Genomics* **14**, 774 (2013).
53. Guo, W. et al. CGmapTools improves the precision of heterozygous SNV calls and supports allele-specific methylation detection and visualization in bisulfite-sequencing data. *Bioinformatics* **34**, 381–387 (2018).
54. Krueger, F. & Andrews, S. R. SNPsplit: Allele-specific splitting of alignments between genomes with known SNP genotypes. *F1000Res* **5**, 1479 (2016).
55. Schutsky, E. K. et al. Nondestructive, base-resolution sequencing of 5-hydroxymethylcytosine using a DNA deaminase. Nat Biotechnol (2018).
56. Guo, F. et al. Active and passive demethylation of male and female pronuclear DNA in the mammalian zygote. *Cell Stem Cell* **15**, 447–459 (2014).
57. Shen, L. et al. Tet3 and DNA replication mediate demethylation of both the maternal and paternal genomes in mouse zygotes. *Cell Stem Cell* **15**, 459–471 (2014).
58. Adenot, P. G., Mercier, Y., Renard, J. P. & Thompson, E. M. Differential H4 acetylation of paternal and maternal chromatin precedes DNA replication and differential transcriptional activity in pronuclei of 1-cell mouse embryos. *Development (Cambridge, England)* **124**, 4615–4625 (1997).
59. Wang, H. et al. One-step generation of mice carrying mutations in multiple genes by CRISPR/Cas-mediated genome engineering. *Cell* **153**, 910–918 (2013).
60. Yang, H. et al. One-step generation of mice carrying reporter and conditional alleles by CRISPR/Cas-mediated genome engineering. *Cell* **154**, 1370–1379 (2013).
61. Yang, H., Wang, H. Y. & Jaenisch, R. Generating genetically modified mice using CRISPR/Cas-mediated genome engineering. *Nat. Protoc.* **9**, 1956–1968 (2014).
62. Dai, H. Q. et al. TET-mediated DNA demethylation controls gastrulation by regulating Lefty-Nodal signalling. *Nature* **538**, 528-+ (2016).
63. Coope, G. J. et al. Predictive blood glucose lowering efficacy by Glucokinase activators in high fat fed female Zucker rats. *Br. J. Pharmacol.* **149**, 328–335 (2006).
64. Grimsby, J. et al. Allosteric activators of glucokinase: potential role in diabetes therapy. *Science* **301**, 370–373 (2003).
65. Wang, P. et al. Effects of a Novel Glucokinase Activator, HMS5552, on Glucose Metabolism in a Rat Model of Type 2 Diabetes Mellitus. *J Diabetes Res* **2017**, 5812607 (2017).
66. Gorman, T. et al. Effect of high-fat diet on glucose homeostasis and gene expression in glucokinase knockout mice. *Diabetes Obes Metab* **10**, 885–897 (2008).
67. Johnson, D. et al. Glucose-dependent modulation of insulin secretion and intracellular calcium ions by GKA50, a glucokinase activator. *Diabetes* **56**, 1694–1702 (2007).
68. Wei, P. et al. Effects of glucokinase activators GKA50 and LY2121260 on proliferation and apoptosis in pancreatic INS-1 β cells. *Diabetologia* **52**, 2142–2150 (2009).

Acknowledgements We thank B. Han for providing APOBEC3A deaminase, Z. Shen for anti-GCK antibody; S. Hong, C. Zhou and G. Xu for technical assistance in embryo manipulation; M. Cai for data analysis; L. Shen, Y. Pan, H. Wang, Q. Xu, L. Xu, J. Xue, Z. Zhou, X. Liu, C. Xu, J. Zhang and H. Yang for discussions; and T. Gu, L. Rui, X. Li, Y. Chen, H. Fan and S. Xuan for critical reading of the manuscript. This work is supported by the National Key R&D Program of China (2017YFC1001300 to H.H.; 2018YFA0800302 to G.-L.X.; 2017YFC1001301 to Y.-R.D.; and 2018YFC1004402 to J.S.), the National Science Foundation of China (82088102 to H.H.; 81661128010 to H.H.; 31991163 to G.-L.X.; 31671569 to J.S.; and 81971458 to G.D.), Shanghai Jiao Tong University, CAMS Innovation Fund for Medical Sciences (CIFMS) (2019-I2M-5-064 to H.H.), Collaborative Innovation Program of Shanghai Municipal Health Commission (2020CXJQ01 to H.H.), Technology Innovation Action Plan Hong Kong, Macao and Taiwan Science and Technology Cooperation Project (19410760100 to H.H.), Shanghai Frontiers Science Research Base of Reproduction and Development (to H.H.) and Zhejiang Provincial Natural Science Foundation of China under Grant (LQ21H040005 to B.C.).

Author contributions H.H. conceived the original idea and, together with G.-L.X. J.S., B.C. and Y.-R.D. designed the experiments. Experiments were performed by B.C. with the help of: Y.-R.D. for the experiments associated with oocytes and RT–qPCR; H.Z. for mouse modelling, phenotyping and human sample collection; M.-L.S. for the experiments associated with TET3 rescue, allele-specific methylation measurement and mouse modelling; C.W. for Smart-seq2 and PBAT library building, data analysis and bisulfite sequencing; Y.C. for islet phenotyping and mouse modeling; H.P. for pyrosequencing analysis; G.D. for supervising human sample collection; J.G. for micromanipulation; Y.T. for human oocyte IVM; and Z.-M.X. for animal housing and genotyping. L.J., Y.Z. and C.Y. assisted with mouse modelling and phenotyping. P.R.F. assisted with interpretation of data. X.T., P.L., F.Z., Q.Z., L.W., D.L., Y.Y., L.J., S.Z., Y.Z., X.L. and Y.W. recruited the patients and collected the human samples. B.C., Y.-R.D., P.R.F., G.-L.X. and H.H. wrote the manuscript with contributions from all other authors.

Competing interests The authors declare no competing interests.

Additional information

Supplementary information The online version contains supplementary material available at https://doi.org/10.1038/s41586-022-04756-4.

Correspondence and requests for materials should be addressed to Guo-Liang Xu or Hefeng Huang.

Peer review information *Nature* thanks Evan Rosen and the other, anonymous reviewers for their contribution to the peer review of this work.